Eur Biophys J (2006) 35:713–719
DOI 10.1007/s00249-006-0079-1

BIOPHYSICS LETTER

Cell migration through small gaps

Claudia A. Brunner · Allen Ehrlicher · Bernd Kohlstrunk · Detlef Knebel · Josef A. Käs · Michael Goegler

Received: 22 March 2006 / Revised: 10 May 2006 / Accepted: 15 June 2006 / Published online: 27 July 2006

Abstract Cell motility is a fundamental process associated with many phenomena in nature, such as immune response, wound healing, and cancer metastasis. In these processes, cells must squeeze through cell layers, and we characterize this ability to actively produce forces and simultaneously adapt their shapes. We have measured forward forces up to 15 nN that a migrating keratocyte was able to generate, in order to adjust its shape and successfully force its way under and past an obstacle. We also observed that 34 nN was capable of stalling the cell's forward motion. Furthermore, we measured that under compression stresses up to 1,165 pN/μm^2 (1,165 Pa), cell morphology, and velocity remained unchanged. Additionally, we found that keratocytes were able to compress themselves up to 80% vertically in order to squeeze through a gap as small as 500 nm.

Abbreviation

AFM Atomic force microscope
IRM Interference reflection microscopy

Authors Claudia A. Brunner, Allen Ehrlicher, and Michael Goegler have contributed equally to this work.

C. A. Brunner · A. Ehrlicher · B. Kohlstrunk · J. A. Käs (✉) · M. Goegler
Institute for Soft Matter Physics, University of Leipzig, Linnéstrasse 5, 04103 Leipzig, Germany
e-mail: jkaes@physik.uni-leipzig.de

D. Knebel
JPK Instruments AG, Bouchéstrasse 12, 12435 Berlin, Germany

Introduction

A common scientific view of cell migration is cells freely moving on a two-dimensional flat surface of a Petri dish. In reality, however, cells generally move through dense tissue where they are in contact with other cells, requiring them to squeeze, and force their way through. Under these conditions a cell must not only have the ability to adapt and restructure its shape at any time but also dynamically exert forces against its surrounding matrix, and withstand the stresses from other cells. These abilities are mediated by the cytoskeleton, a viscoelastic active polymer network, which supports a cells' structure but remains flexible. It is able to generate forces via molecular motors, such as myosin or kinesin (Finer et al. 1994; Block et al. 2003), and by polymerization of proteins, like actin or microtubules (Theriot 2000).

One extreme example for the importance of force generation and maximum flexibility of the cytoskeleton in cell migration is the process of inflammation. Leukocytes bind to adhesion molecules at the cell wall of a blood vessel, flatten out, squeeze through small gaps between the endothelial cell wall, and migrate into the surrounding tissue (Springer 1994). Another example is tumor metastasis where tumor cells leave the main tumor, migrate toward the endothelial cell wall of a blood vessel, and squeeze through. Once in the blood stream it is possible for metastatic tumor cells to spread into different areas of the body to form secondary tumors (Hanahan and Weinberg 2000).

This ability to generate and withstand forces during migration by overcoming obstacles or squeezing through small gaps between cells is the focus of this letter. We put a polystyrene bead (~ size of a cell)

glued to a cantilever tip of an atomic force microscope (AFM) as an obstacle in front of a migrating cell. The cell crawled underneath the bead, pushed it up bending the cantilever, and squeezed through as depicted in Fig. 1. We observed the movement of the cell and measured the forces at the leading edge of the cell and at the cell body.

The cells under investigation are fish keratocytes, fast moving (several μm/min) cells, which maintain nearly constant velocity, and a half-moon morphology during migration. They are commonly studied in cell motility because of their rather conserved shape and their directionality in motion (usually perpendicular to their long axes), which makes them the perfect test case for our study, despite their largely two-dimensional movement in vivo.

Experimental

Keratocyte culture

Primary goldfish epithelial keratocytes were cultured in Dulbecco's modified Eagle's medium (DMEM) (Sigma D6429, St. Louis, MO, USA) supplemented with 20% fetal bovine serum (ATCC), 10 mM HEPES (Sigma), and 100 U/ml penicillin-streptomycin (Sigma P0781).

Light microscopy

An inverted video microscope (Leica DM IRB) allowed positioning of the cantilever tip and imaging of cell movement in phase contrast (Leica 40 × Ph2) as well as in interference reflection microscopy (IRM) (Leica 63 × Ph3) (Izzard and Lochner 1976). The IRM technique permitted us to observe regions close to the substrate. When visualized with IRM, regions in contact with the substrate appear darker than not adhered regions, as is seen in Fig. 2. By inhomogeneously illuminating the sample, reflections from the cantilever were eliminated but the bead's position and the cell's contour were still visible.

While phase contrast was mainly used for illustration and positioning of the cantilever, analysis, and evaluation were done with the more detailed IRM images.

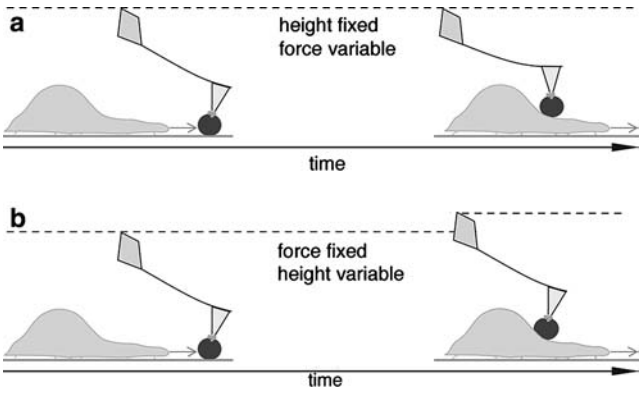

Fig. 1 Illustration of the experiment. A polystyrene bead (*dark gray*) glued to a cantilever-tip of an AFM was positioned on the substrate in front of a migrating cell. The cell moved toward the bead, crawled under it, and pushed the cantilever upwards. In constant height mode (**a**), the *z*-piezo of the AFM was fixed, the vertical deflection of the cantilever was recorded, and calculated into force, whereas in constant force mode (**b**), the piezo's *z* was not fixed and its movement was recorded

Atomic force microscopy

Setup

A commercial AFM (Nano Wizard, JPK Instruments AG, Berlin, Germany) was mounted on an inverted video microscope allowing for all common light microscopy techniques.

Polystyrene beads with a 1.5–3 μm radius R (Seradyn uniform microparticles, infinitely rigid compared to the cell) were glued to cantilever tips (NanoWorld Pointprobe CONT sensors and BSI sensors, Neuchatel, Switzerland) to provide a well-defined probe geometry and avoid puncturing the cell (Mahaffy et al. 2004).

The cantilever spring constant k_c was determined by the thermal noise method (Butt and Jaschke 1995) and by calibration against a cantilever of known spring constant (Tortonese 1997). The torsional spring constant was determined from theoretical considerations with $k_\phi = k_c{*}2L^2/(3{*}(1+\mu))$, where L is length of the cantilever, μ is the Poisson ratio of the cantilever ($\mu = 0.25$) (Green et al. 2004). Initial pushing force measurements were made with elastically compliant (k_c ~15 mN/m) cantilevers, whereas attempts to stop cells were performed with stiffer (k_c ~130 mN/m) cantilevers.

Elasticity measurements and indentation depth calculation

The cells' elasticities were measured for keratocytes at the lamellipodia and cell bodies. The local ''elastic constant'', $k = E/(1–\nu^2)$, with Young's modulus E, and the Poisson ratio ν, was derived from force–distance curves using the Tu or the Chen model, which build on the Hertz model by correcting for the finite thickness of thin samples (Mahaffy et al. 2004). The Tu model best fits regions poorly adhered to the substrate, while the Chen model is valid for regions strongly attached to

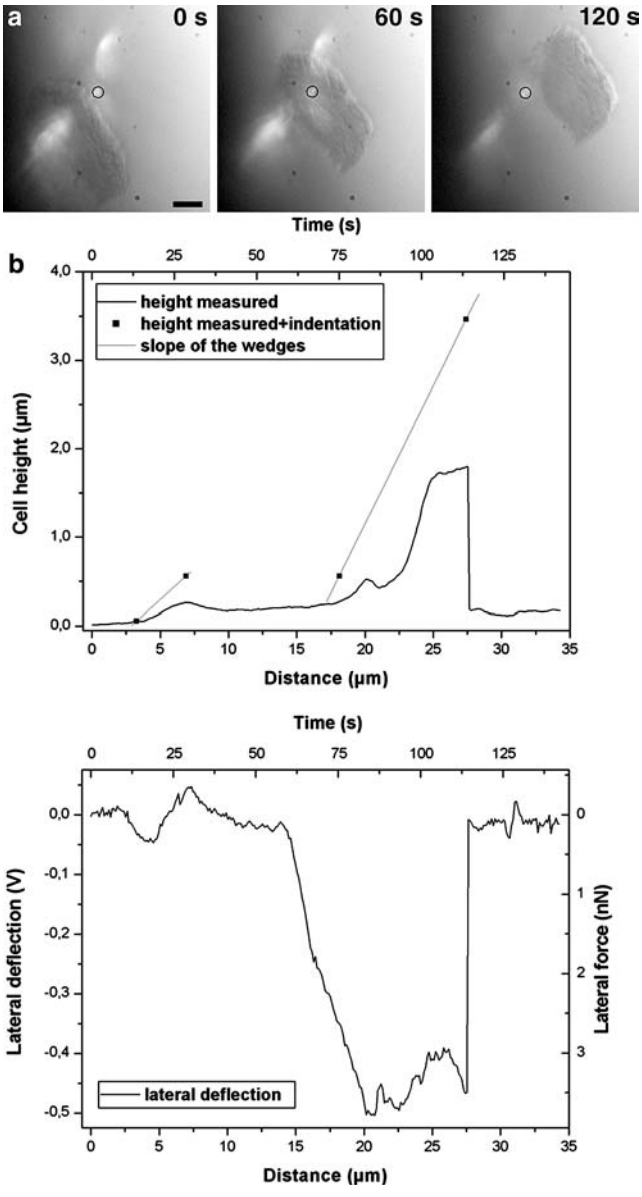

Fig. 2 Experimental data for a keratocyte with constant force on (setpoint is 4.1 nN, k_c = 15.9 ± 2.1 mN/m, R = 1.5 ± 0.1 µm), resulted in a maximum downward stress of 1,165 ± 292 pN/µm^2 (1,165 ± 292 Pa). The *upper panel* shows a series of consecutive IRM images during the measurement (scale bar = 10 µm). Time in seconds is given in the upper right corner of each image and corresponds to the time scale in the respective graphs below. The bead pushing on the substrate is outlined in *black* for clarity. In the *middle panel*, the indentation depths δ were added to the measured height signal, resulting in the undeformed height of the cell (*squares*). Straight *gray lines* represent the corrected slopes for the leading edge of the lamellipodium and the lamellipodial back, which are required for our wedge model calculation. The *lower panel* shows the lateral deflection (k_ϕ = 410 ± 62 pNm/rad). The total forward force was measured from the combined lateral and vertical deflections, and was 1.0 ± 0.3 nN at the lamellipodium and 5.4 ± 0.9 nN at the cell body, corresponding to forward stresses of 610 ± 155 pN/µm^2 (610 ± 155 Pa) and 720 ± 90 pN/µm^2 (720 ± 90 Pa), respectively

the substrate. In recent studies these techniques have been proven to give the most accurate k values (Mahaffy et al. 2004), in contrast to other techniques, which yield too high values. We measured a typical k value for the cell body of 0.67 ± 0.18 and 1.28 ± 0.45 kPa for the lamellipodium (mean ± SD, n = 10) using either the Tu or the Chen model according to the best data fit using a look-up table. These elasticities are lower than those reported previously (10–55 kPa), however, these earlier measurements did not account for substrate stiffness, and are understood to be overestimates (Laurent et al. 2005).

From the elasticity one can calculate the indentation depth, which is necessary to know the undeformed cell height in an actual pushing force experiment. While we calculated the cell elasticities using the accurate Tu or Chen model, we used the simpler Hertz model, $F_{bead} = 4/3*k*R^{1/2}*\delta^{3/2}$, and Hertz k values (cell body: k = 1.16 ± 0.16 kPa, lamellipodium: k = 2.64 ± 0.74 kPa, n = 10) to determine the indentation depth δ. This can be done since numerical corrections in the Tu or Chen model, $F_{Tu,Chen} = F_{bead}*correction_{Tu,Chen}$, are undone when calculating δ with the Tu or Chen k-values in the Tu or Chen model.

For large indentations (on the order of a bead radius), axial strains can be as high as a 100%, and a linear elastic behavior of the cell is debateable (Gardel et al. 2004). To test this problem, a cell body was deeply indented by the cantilever four times with increasing forces, even including larger forces (~25 nN) than the upward forces measured in most of the actual experiments, and the ''elastic constants'' of the cell were determined. We compensated for substrate stiffness, as well as cell adherence when calculating our elasticities, as described previously (Mahaffy et al. 2004). Our calculated elasticities showed no dependence on the applied force (as shown in Fig. 4c), thus validating our linear approximation of the cell.

For the thin lamellipodium and strong indentations, however, nonlinear substrate effects arise which cannot be corrected for in the indentation depth calculations. In these cases, another method was applied which used an average height of the undeformed lamellipodium of 560 ± 110 nm (mean ± SD, n = 18) as a baseline. The actual indentation depth is then given by subtracting the measured signal at the lamellipodium in the experiment from the determined baseline of 560 nm.

Data analysis

Since the cantilever is essentially a spring, which can bend (vertical deflection) and rotate (lateral deflection),

we measured both signals to get the total force of a cell. During an experiment vertical and lateral deflection signals (V_V and V_L, respectively) were read out and recorded every 2 s. Knowing the sensitivity s (nm/V and rad/V, respectively) and the spring constants k (mN/m and Nm/rad, respectively) of the cantilever allowed the conversion of the vertical signal into force and height and of the lateral signal into torque τ. The lateral force can be evaluated using the general relation $F_L = \tau/l$, where $\tau = s_\phi * k_\phi * \Delta V_L$, and l is the moment arm which is here tip length plus a certain fraction of the bead diameter, depending on the indentation depth.

Velocity and position of the cell were determined via analysis of recorded phase contrast or IRM images. With the obtained cell velocity v, the translocation distance between measurement time points was calculated.

The calculated indentation depth δ of the bead was added to the vertical deflection, which resulted in corrected slopes at the lamellipodium and at the cell body, allowing the calculation of the forward-pushing force. We also calculated the stresses based on the contact area of the bead, as determined by the indentation depth.

Results and discussion

Here we present measurements of the pushing forces generated at the leading edge of the lamellipodium and the cell body while a cell is squeezing its way past an obstacle. A polystyrene bead glued to an AFM cantilever-tip was pushed with a preset force against the substrate, acting as an obstacle in front of a migrating keratocyte. The keratocyte approached the bead and pushed it up as the cell passed underneath, bending the cantilever as shown in Fig. 1. The bending and twisting of the cantilever was detected as vertical and lateral deflection signal, respectively, and converted into height and force (see section Experimental).

A typical experiment is shown in Fig. 2. The behavior of the cell when influenced by the bead (outlined in black) was observed with IRM, and is shown in the upper panel. In this example, the keratocyte passed underneath the bead from down left to top right with a mean velocity of 14.5 ± 0.3 μm/min. General morphology and motion remained unchanged during the measurement. The height signal and the lateral deflection converted into force as functions of time and distance are shown in the lower panels of Fig. 2. Both signals correlate appropriately with the observed motion of the cell seen with IRM.

The cell was locally elastically deformed by at least 40% and generated upward stresses up to 1.2 ± 0.3 nN/μm^2, which is equivalent to 1.2 ± 0.3 kPa, and moved past the bead.

In other experiments where cells successfully squeezed through underneath the bead without changing their velocities, upward stresses of up to 1.5 ± 0.4 nN/μm^2 were measured. The cells were locally deformed up to 80% of their normal height and managed to squeeze through gaps ranging from 300 to 2,800 nm depending whether or not the nucleus went directly underneath the bead.

In another experiment (Fig. 3), the cantilever pushed with a preset force of 65 ± 9 nN on the substrate and the cell was not able to squeeze underneath the bead. The translocation of this keratocyte, originally moving with 5.4 ± 0.1 μm/min from bottom to top (Fig. 3 upper panel), was stopped. The lamellipodium stalled locally and split at the bead (outlined in black). Subsequently, the whole cell did not generate enough force to overcome the obstacle. Instead the cell restructured and turned around, moving then in opposite direction from top to bottom with the very

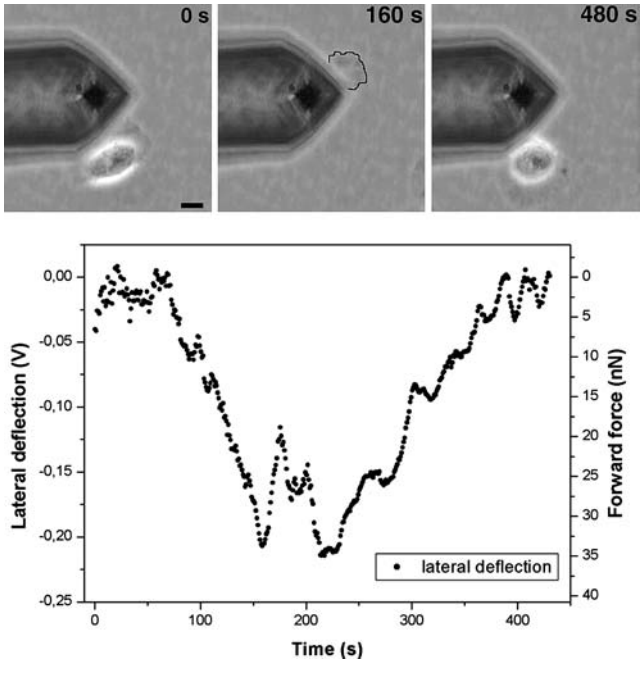

Fig. 3 Stall force experiment. A keratocyte was stopped with a lateral force of 34 nN and a vertical force of 65 nN (k_c = 100 ± 20 mN/m, R = 2.8 ± 0.1 μm). *Upper panel* shows consecutive phase contrast images of the experiment (scale bar = 10 μm). Time is given in the upper right corner and corresponds to the time given in the *lower panel*. In the image at 160 s the peripheral lamellipodial flank is outlined in *black* for clarity. The *lower panel* shows the lateral deflection and force (k_ϕ = 10.8 ± 1.6 nNm/rad)

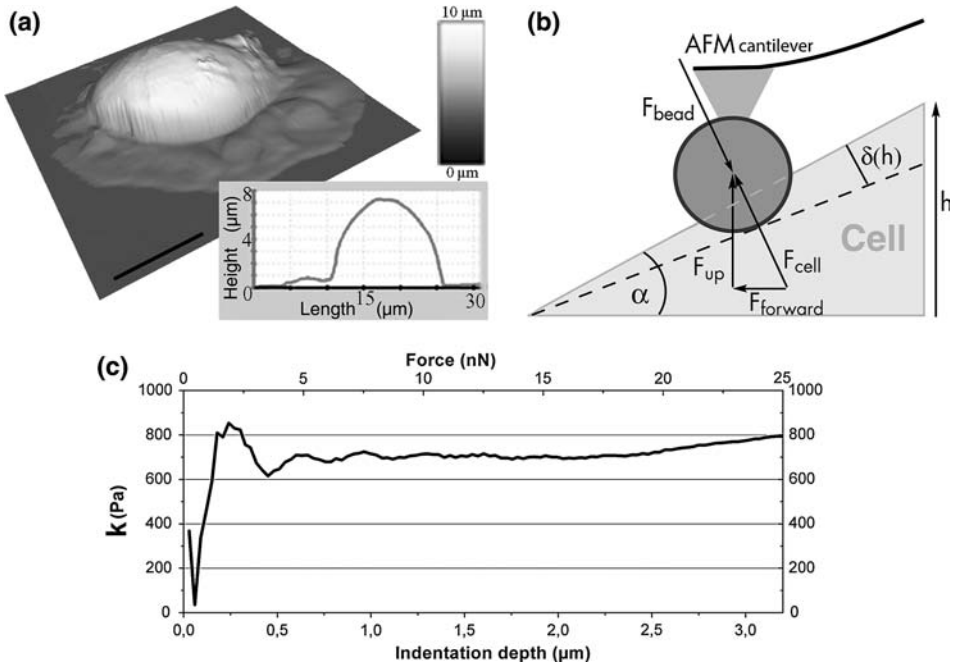

Fig. 4 Topography of a keratocyte, ''elastic wedge model'', and dependence of k on force. (**a**) Three-dimensional height profile of a migrating keratocyte fixed with paraformaldehyde, taken with a 4.2 ± 0.6 µm bead on the cantilever tip. The flat region shows the lamellipodium, the high region the cell body. The *inset* shows a cross-section of the cell height. (**b**) ''Elastic wedge model''. An AFM-attached polystyrene bead was pushed up and indented the cell as the cell moved forward. Steep regions of the cell, such as the leading edge of the lamellipodium, and of the cell body, were modeled as elastic wedges. The real cell height was corrected with the indentation depth δ, which increased with rising cell height h (in constant height mode). The force generated by the cell F_{cell} was balanced by the force exerted by the cantilever F_{bead}. The vertical deflection or upward force F_{up} detected by the AFM was calculated into a forward-pushing force $F_{forward}$ using the slope α of the wedge. Friction and bead-cell adhesion were neglected in our model, which resulted in a lower bound for $F_{forward}$. (**c**) Elastic constant k as a function of indentation force at a 5.7 µm high cell body. Since k only varied 14%, while the force changed 500% (from 5 to 25 nN), we determined the elasticity to be force-independent, and thus used linear elasticity theory

same velocity of 5.4 ± 0.1 µm/min. The vertical deflection only shows noise, which reflects the unsuccessful try of the cell to squeeze under the bead and push the cantilever out of its path (data not shown). In the lateral direction, the cell clearly twisted the cantilever, which corresponds to a force pushing in the direction of motion (Fig. 3 lower panel).

Keratocytes, in contrast to phagocytosing macrophages, do not lift up from the substrate to ingest particles, such as bacteria or beads. Therefore actively generated upward forces are unlikely to be the cause for the measured signal in the experiments. In the following it will be shown that solely the forward-pushing forces generated by a cell are enough to explain the observed upward forces.

A typical topographical profile encountered by the bead is shown in Fig. 4a. The thin region corresponds to the lamellipodium, and the high region to the cell body. The cell's cross-section (Fig. 4a, inset) shows an increase in height at the front of the lamellipodium, and at the transition zone between lamellipodium and cell body. We used these areas to measure the forward forces, since in these regions the migrating cells continuously increased the cantilever deflection. We modeled these relevant slopes as elastic wedges. Since cells are elastically compliant, the bead on the cantilever indents the cell. The force exerted on the cell by the cantilever increases with rising cell height, and consequently the indentation depth also increases for a fixed z-piezo position. To calculate the purely active force component, we corrected for the elastic contribution of the cell by adding the indentation depth to the measured vertical deflection of the cantilever (Fig. 4b, dashed line). Thus, we can calculate the actual cell height (Fig. 4b, solid line), and correct the wedge slope (see also Fig. 2). The forward force was then calculated with the measured upward force (vertical deflection) and the corrected angle α of the wedge using $F_{forward} = F_{up} * \tan \alpha$.

Cells crawling perpendicular to the cantilever caused also a considerable torsion of the cantilever, again mainly in the regions of increasing cell height. This lateral deflection allowed a direct measurement of the forward-pushing force (see section Experimental).

Since the torque τ was generated at the indented area of the cell, we took the fraction of the indented bead area opposing the direction of motion and approximated the lateral pushing force with $F_{pl} = \tau/(d\text{-}\delta/2)$, where d is maximum moment arm (tip length plus bead diameter) and δ is the indentation depth of the bead. Superposition of lateral and vertical measured forward forces led to the total forward-pushing force of a cell.

In most experiments either the lateral or vertical component dominated, depending on the direction of the cells' motion with respect to the cantilever but also on the opposing stress and thus on the bead dimension and the preset vertical force used. In general, small stresses (big beads, small vertical force) led to very clear vertical signals and small torsions and allowed an analysis based mostly on the soft wedge model. Higher stresses, however, caused deep indentations and sometimes led to morphological changes of the cell. In these cases, the lateral deflection signal detected the strongest contribution of the forward-pushing force. Here, the limit of the wedge model was exceeded and contributions from the vertical signal could not be evaluated. The measured lateral and vertical components of the forward-pushing force were the same order of magnitude.

The results for the measured forward force can be separated into two categories: forces measured at the lamellipodial front, and those measured at the cell body. The forces measured at the same categorized regions with different cells were consistent. Consecutive measurements of specific individual cells with the same opposing force were repeatable, demonstrating the robustness of our method. We tested this by measuring the lamellipodium and cell body protrusion forces of two unique cells at two different time points with the same applied force. We found that in all cases the values for each cell and region at different time points were within the error of measurement (~34%). In all of our measurements, forward forces at the lamellipodium ranged from 0.4 to 2.4 nN (210–1,030 pN/μm^2) (n = 8), while forces at the cell body were larger, ranging from about 2.8 to 15 nN (410–1,390 pN/μm^2) (n = 12). These measured forward forces are reasonable and on the same order as predicted (Mogilner and Oster 2003). Within this force range we did not observe any obvious changes in cell's morphology or velocity. Our observations clearly exceed the results of Bohnet et al. where they found that a weak force of a few piconewtons, induced by a fluid flow, is enough to lift up and stall the leading edge of a lamellipodium. They suggest, however, that they do not stall the active pushing force but disrupt weak nascent adhesion points at the leading edge (Bohnet et al. 2006).

Joanny et al., predicted interesting velocity behavior depending on the location of the applied force (Joanny et al. 2003). Our observations showed no obvious change in cell velocities within our range of applied forces.

Our measured stall forces for whole keratocytes (see Fig. 3) of 34 ± 6 and 85 ± 15 nN are in agreement with those reported earlier by Oliver et al., who used the deflection of an adhered micro-needle to oppose the motion of a keratocyte and measure the net traction force (~45 nN) of the cell (Oliver et al. 1995). Despite the difference in techniques, in both cases the entire cell's force was stopped using a local obstruction; thus the results are directly comparable. In general, when cells crawl through tissue they must squeeze between other cells. Our observations show that even a keratocyte cell, which is typically found in quasi-two-dimensional layers, is strong enough to generate substantial forward-pushing forces and adapt its shape while squeezing through gaps.

Acknowledgments The authors thank JPK-Instruments for their help. This work was supported by the EU project ''Active Biomimetic Systems'', and the Deutsche Forschungsgemeinschaft (DFG KA 1116/3–2).

References

Block SM, Asbury CL, Shaevitz JW, Lang MJ (2003) Probing the kinesin reaction cycle with a 2D optical force clamp. Proc Natl Acad Sci USA 100:2351–2356

Bohnet S, Ananthakrishnan R, Mogilner A, Meister JJ, Verkhovsky AB (2006) Weak force stalls protrusion at the leading edge of the lamellipodium. Biophys J 90:1810–1820

Butt H-J, Jaschke M (1995) Calculation of thermal noise in atomic force microscopy. Nanotechnology 6:1–7

Finer TJ, Simmons RM, Spudich JA (1994) Single myosin molecule mechanics: piconewton forces and nanometre steps. Nature 368:113–119

Gardel ML, Shin JH, MacKintosh FC, Mahadevan L, Matsudaira P, Weitz DA (2004) Elastic behavior of cross-linked and bundled actin networks. Science 304:1301–1305

Green CP, Lioe H, Cleveland JP, Proksch R, Mulvaney P, Sader JE (2004) Normal and torsional spring constants of atomic force microscope cantilevers. Rev Sci Instrum 75:1988–1996

Hanahan D, Weinberg RA (2000) The hallmarks of cancer. Cell 100:57–70

Izzard CS, Lochner LR (1976) Cell-to-substrate contacts in living fibroblasts: an interference reflexion study with an evaluation of the technique. J Cell Sci 21:129–159

Joanny JF, Jülicher F, Prost J (2003) Motion of an adhesive gel in a swelling gradient: a mechanism for cell locomotion. PRL 90:1681021–1681024

Laurent VM, Kasas S, Yersin A, Schaffer TE, Catsicas S, Dietler G, Verkhovsky AB, Meister JJ (2005) Gradient of rigidity in the lamellipodia of migrating cells revealed by atomic force microscopy. Biophys J 89:667–675

Mahaffy RE, Park S, Gerde E, Käs J, Shih CK (2004) Quantitative analysis of the viscoelastic properties of thin regions

of fibroblasts using atomic force microscopy. Biophys J 86:1777–1793
Mogilner A, Oster G (2003) Polymer motors: pushing out the front and pulling up the back. Curr Biol 18:721–733
Oliver T, Dembo M, Jacobson K (1995) Traction forces in locomoting cells. Cell Motil Cytoskel 31:225–240
Springer TA (1994) Traffic signals for lymphocyte recirculation and leukocyte emigration: the multistep paradigm. Cell 76:301–314
Theriot JA (2000) The polymerization motor. Traffic 1:19–28
Tortonese M (1997) Cantilevers and tips for atomic force microscopy. IEEE Eng Med Biol Mag 16:26–27